Influence of Environment and Light-Stress on the Optoelectronic Properties of Triple-Cation Perovskite Thin Films

Hung-Ju Lin, Stefania Cacovich, Amelle Rebai, Jean Rousset, Christophe Longeaud

Influence of Environment and Light-stress on the Opto-Electronic Properties of Triple-Cation Perovskite Thin Films

Hung-Ju Lin[1], Stefania Cacovich[1], Amelle Rebai[1], Jean Rousset[1,3], Christophe Longeaud[1,2]*

[1] Institut Photovoltaïque d'Île-de-France (IPVF), 18 Bd Thomas Gobert, 91120 Palaiseau, France

[2] GeePs, CNRS, Centrale Supelec, Université Paris-Saclay, 91192 Gif-sur-Yvette Cedex, France

[3] EDF R&D, 18 Bd Thomas Gobert, 91120 Palaiseau, France

KEYWORDS: Triple-cation perovskite, photoluminescence, SSPG, transport properties, aging influences

ABSTRACT. In this work we study the transport properties of triple-cation halide perovskite thin films and their evolution when exposed to air or vacuum, and after light-soaking. Transport parameters were investigated by steady state dark and photocurrent methods as well as by the steady state photocarrier grating experiment (SSPG) from which the ambipolar diffusion length of thin film materials is estimated. Combined with other characterization measurements, such as photoluminescence and Fourier transform photocurrent spectroscopy, these techniques demonstrate that air plays an important role in the passivation of the surface trap states of the perovskite films. The competition between passivation and degradation of the films under light-soaking was also deeply investigated. Moreover, we show that the

degradation of the transport parameters upon light-soaking could be linked mainly to a degradation of the carrier mobility instead of their lifetime.

1. INTRODUCTION

Among the material candidates to produce low-cost photovoltaic devices, hybrid inorganic-organic perovskite absorbers have emerged as one of the most promising technology.[1-3] In just a decade, perovskite solar cells (PSCs) efficiency has rapidly increased from 3.8%[4] to a remarkable value over 25%[5] that is already comparable with that of commercial c-Si solar cells. These impressive achievements also opened new applications into other fields such as light-emitting diodes,[6] lasers,[7, 8] and photo-detectors.[9, 10]

Beyond high conversion efficiency of PSCs, their stability under outdoor conditions is still an issue and can be a barrier for long term applications, even though it was demonstrated that PSCs are stable for thousands of hours in laboratory tests.[11] Generally speaking, environmental factors coming from atmosphere, light, moisture, and thermal effects, have been proved to be detrimental to the stability of organic devices.[12, 13] The same factors can be also critical for inorganic-organic perovskites (PVK).[14, 15] For example, degradation can be caused by fast oxygen diffusion into perovskite films.[16] However, there is no clear interpretation of the observed degradation and the relevant mechanisms remain unclear. Indeed, in some experiments, the atmosphere has been pointed out as being beneficial to transport properties, where it could play a role in passivation of perovskite traps, leading to an enhancement of the photoluminescence (PL).[17, 18] This behavior was explained by the formation of superoxide species (O_2^-) at iodide vacancies while the films are exposed to atmosphere under light illumination.[19] Another interpretation also mentioned a similar mechanism of passivation of deep/ shallow traps through oxygen diffusion.[20] However, to our knowledge, there is still no relevant proof and direct observation of it, especially on

perovskite films containing double (methylammonium: MA and formamidinium: FA) or triple-cation (MA, FA, and Cs). In this study we have concentrated on triple-cation PVK because it is known as state of the art absorber with enhanced stability and performances.[21]

Here, we report systematic in-situ studies on perovskite films containing triple-cation (MA, FA, and Cs) in order to investigate the dynamic changes of their transport properties and potential passivation, combining aging tests under different environment conditions (air and vacuum). For this purpose, we have combined optical characterization techniques, *i.e.* photoluminescence excited by continuous wave lasers and Fourier transform photocurrent spectroscopy (FTPS),[22, 23] and electronic characterization techniques, *i.e.* steady state photoconductivity (SSPC) and steady state photocarrier grating (SSPG).[24] Moreover, the photoluminescence experiments were performed under two different laser wavelengths (470 nm and 670 nm) in order to extract information from different excitation depths in perovskite film, from near surface to whole bulk. With this procedure, we were able to distinguish between the surface and the bulk contribution to the PL signal. As far as the electronic properties are concerned, the SSPG technique provides a direct access to the ambipolar diffusion length (L_d). In most of the techniques found in the literature, the diffusion length is determined by collecting mobility and lifetime results in two different experiments. However, the final results may be altered by the fact that the studied material may be not in the same state in each experiment or is not under a steady state illumination, as underlined by Hodes and Kamat.[25] Besides, combination of different methods, *e. g.* photoluminescence lifetime and time of flight, does not provide a fast and systematic means of measurement of the diffusion length as shown in Ref. [26]. In contrast, the SSPG method proposed first by Ritter *et al.* for studying L_d in photoconductive insulators,[24] provides a fast, direct, and accurate experiment to study the carrier ambipolar diffusion length. Moreover, it has been proved to be suitable for many materials (for a review see Ref. [27]), and it was also shown that it could be applied to

hybrid perovskites.[28] This technique was recently upgraded into an automated experiment including a cryostat allowing study of materials under different conditions, in air and under vacuum at different temperatures.[29] In addition, it was developed so that the samples can be studied under the same illumination as the SSPC measurements. In this communication, we point out that atmosphere can play an important role for improving L_d and photoconductivity of perovskite films. Furthermore, we also carry out a direct proof of the observation of a competitive relationship between passivation and light-induced degradation.

2. RESULTS

In this study we investigate state-of-the-art triple-cation mixed-halide perovskite thin films ($Cs_x(MA_{0.17}FA_{0.83})_{1-x}Pb(Br_{0.17}I_{0.83})_3$) The preparation and deposition of these films, as well as the characterization techniques we have used, are detailed in the experimental section.

2.1 Optical Properties

2.1.a Influence of air or vacuum

The triple-cation perovskite samples were initially maintained inside a dynamically pumped cryostat under a high vacuum level ($<10^{-5}$ mBar) for a few hours. Then, the vacuum was broken and the PL spectra, either excited by a laser wavelength of 470 nm or 670 nm, were recorded at different time intervals as shown in Figures 1(a) and 1(c) respectively. To limit possible light-soaking effects during the spectra acquisition, the measurements were performed by using a shutter so that the film was illuminated only for few seconds. We shall call this experiment the ON/OFF PL in the following. A large increase of the PL emission intensity can be observed once the perovskite thin film is exposed to air. After 20 min of air exposure, the PL maximum is increased by a factor of ~ 3 and starts to saturate after 3 min when illuminated with the blue laser. The same trend is observed when illuminated with the red laser, although we do not observe the same saturation of the PL intensity. This behavior

suggests that air is not systematically harmful to the PVK properties and can even be helpful as also observed by Brenes and coworkers.[20] To further investigate the environment influence, after exposing the PVK films for 20 min under air, we pumped the cryostat again to observe the PL variation within 20 min under vacuum as shown in Figure 1(b) and 1(d) for the 470 and 670 nm lasers, respectively. Interestingly, the PL results show a fully reversible variation while switching between air and vacuum conditions, the intensity being reduced by a factor ~ 1/3 after 20 min under vacuum, in both illumination conditions tested.

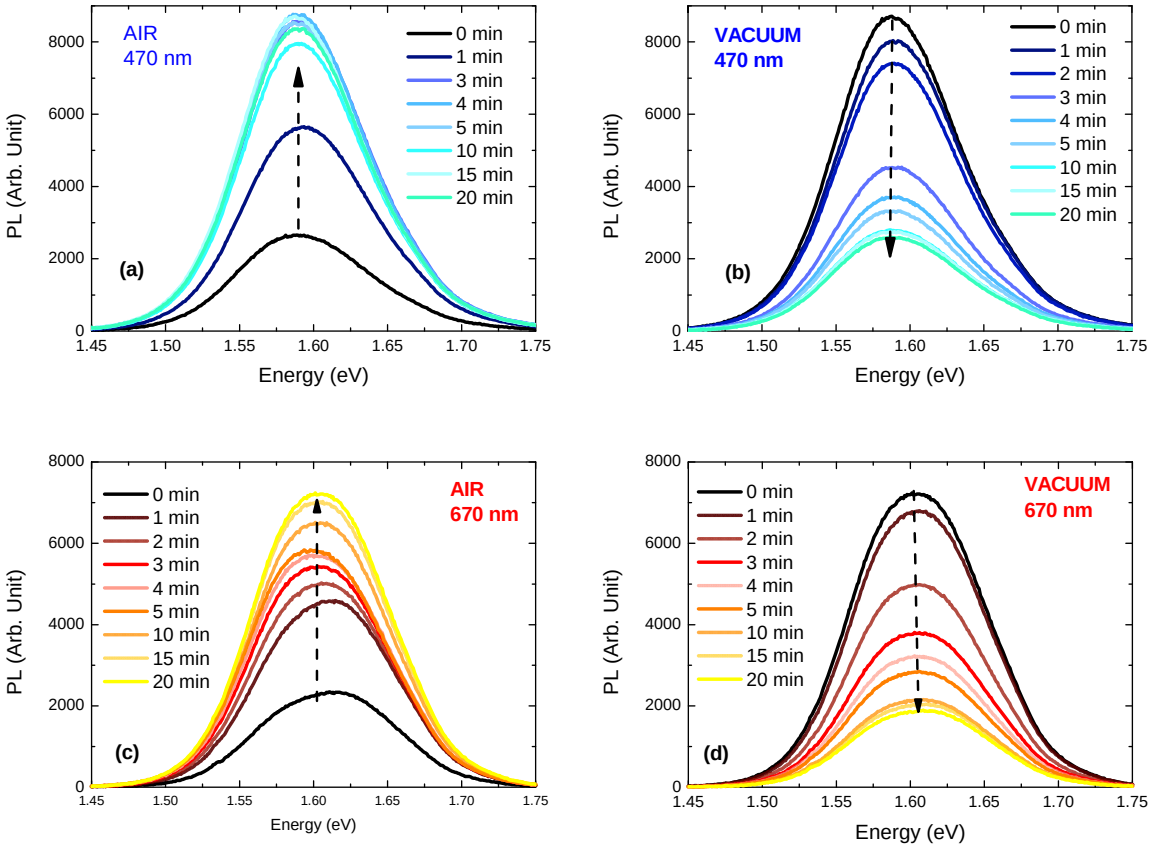

Figure 1. Photoluminescence of PVK films obtained with different laser wavelengths in different environments. In (a) and (b), a 470 nm wavelength laser illuminates PVK films under air and vacuum, respectively. In (c) and (d), a 670 nm wavelength laser was used for PVK films PL excitation under air and vacuum, respectively.

Figs. 1(a) and (c) show that the PL enhancement rate using a 470 nm excitation is faster than with a 670 nm excitation. To point out the kinetics of the PL evolution, the PL maximum value (PL_{max}) has been drawn as a function of exposure time to air or to vacuum. Fig. 2 shows that, with an illumination at 470 nm, PL_{max} rapidly increases and reaches saturation within 2-3 min after exposure to atmosphere, whereas, with an illumination at 670 nm PL_{max} requires a longer air exposure time, even up to 20 min, to reach saturation. However, when switching from air to vacuum condition, the decay rates of both types of excitation look quite similar.

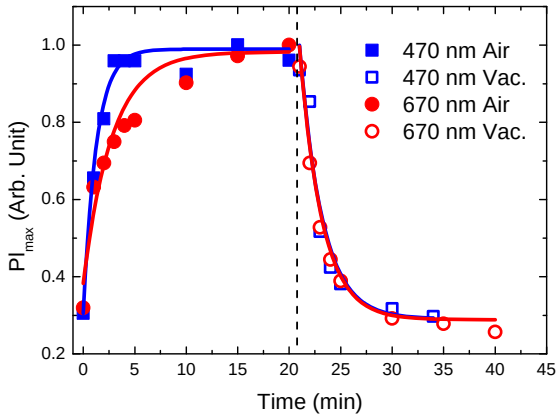

Figure 2. Maximum PL peak values measured with two laser wavelengths (470nm and 670nm) and regularly recorded from vacuum to air (full symbols) and then from air to vacuum (open symbols). The data are normalized to the maximum values of PL_{max}. The full lines represent the fits of the raise and decay of PL_{max} with exponential curves.

The raise and decay of PL_{max} have been fitted with exponential curves to extract the time constants of these evolutions. Full lines in Fig. 2 display the fits of the PL_{max} data (symbols). It can be seen that the raising time constant under air (index *a*) with a 670 nm excitation (index *r*) is $\tau_{ar} \approx 3.0$ min, a value more than two times larger than $\tau_{ab} \approx 1.3$ min obtained under air with a 470 nm laser excitation (index *b*). In contrast, when the films are set back under vacuum (index *v*) the decay time constants, $\tau_{vr} \approx \tau_{vb} \approx 2.2$ min, are equal. The main conclusions we can draw from these analyses are that: i/ atmosphere plays a key role of

improving/passivating the perovskite films as evidenced from the PL enhancement, ii/ the PL intensity evolution takes place within a time scale of a few minutes, and iii/ this phenomenon is reversible.

The same type of experiment was performed with a continuous illumination of the film by the lasers light. The results, shown in the supporting information (Figs. S1, S2 and Table S1), are slightly different from the ones presented above during the ON/OFF PL experiment. The two main differences are a red-shift in the position of the PL maximum intensity when the experiment is performed under air and in the kinetics of the peak intensity evolution. Indeed, the energy position of the PL maximum decreases with time from ~ 1.62 eV to 1.57 eV when the sample is set under air. When the sample is set back under vacuum, PL_{max} energy positions slightly increase but without recovering the original value. In the case of steady illumination, the time constants of the rise of PL_{max} under air are higher than the ones observed for short illumination, reaching values of the order of 8 min for both wavelengths.

2.1.b Influence of light-soaking

The influence of light-soaking on the optoelectronic properties of halide perovskite was then investigated. We light-soaked the samples under air for a long time, up to 21 h, under a white light (high power white LED with a incident power of 44 $mWcm^{-2}$, see Fig. S3). We observed an increase of the PL maximum by a factor of 2 after illumination of the film during 21 h accompanied by a red shift of the peak position from ~ 1.63 eV to ~ 1.60 eV (See Fig. 3(a)). In Fig. 3(b) we display the concomitant evolution of the band gap width measured with the FTPS experiment. The FTPS spectra obtained before and after light-soaking display only the relative variations of α and have been normalized to the same value at 1.75 eV for an easy comparison. It can be seen that, under light-soaking, the gap has shrunk by an amount of ~ 30 meV, the same energy interval as previously observed with the PL peak shift. Though the origin of this gap shrinking remains unclear, it may explain the red-shift of the PL maximum.

However, the PL increase is surprising since it is usually believed that light-soaking results in the creation of recombining states in the gap of thin film semiconductors leading to an increase of the recombination kinetics. On the contrary, this improvement of the photoluminescence suggests a decrease of the density of non-radiative recombination centers.

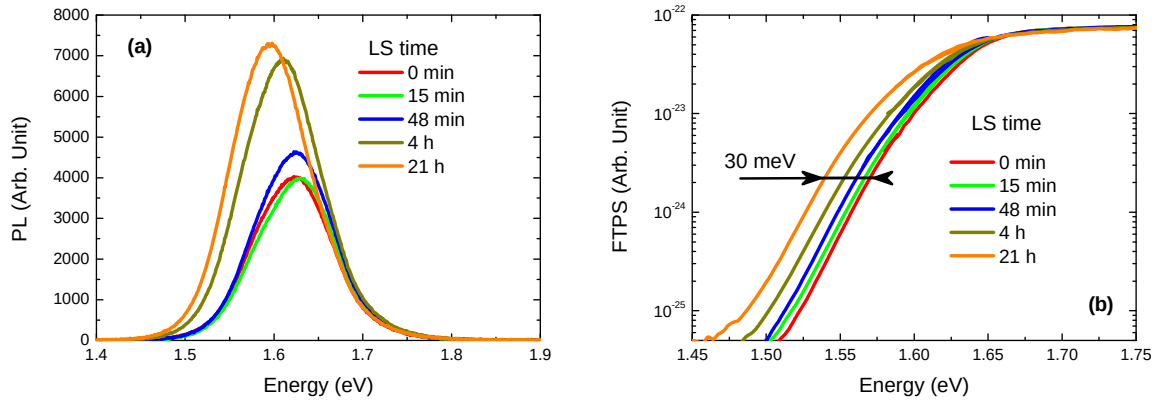

Figure 3. Evolution under light-soaking (a) of the PL spectra, and (b) of the band gap edge, of a PVK thin film.

2.2 Transport properties

In order to study the influence of the environment, air or vacuum, and of the light-soaking on the transport properties of PVK films we have performed SSPC and SSPG measurements under different experimental conditions during one month. Fig. 4 summarizes the results we have obtained at room temperature on one of our samples, the same trends being also observed on other films. The light used to perform these measurements was delivered by a He-Ne laser (632.8 nm) with a power density equal to 12.5 $mWcm^{-2}$ in both experiments, SSPC and SSPG.

When the sample is maintained under air (black symbols) from day 1 after its growth to day 9, L_d and σ_{ph} present almost constant values around 450 nm and 1.4×10^{-4} Scm^{-1} respectively. On the contrary, when the sample is set under vacuum after day 9 (red symbols) we first observe a concomitant decrease of L_d and of σ_{ph}, though a small increase of this latter

appears just after the sample is set under vacuum. Then, with time, we observe a slight improvement of these quantities, but largely less pronounced as when the sample is set back in the air on day 23.

Subsequently, the sample was light-soaked under air for 45 hours leading to decrease of photoconductivity by a factor of 8, from 1.0×10^{-4} to 1.2×10^{-5} Scm^{-1}, whereas the diffusion length is rather constant at a value around 350 nm. Once the sample is set under vacuum, we observe again a decrease of the transport properties (day 29) with a slight recover on day 30.

Remarkably, in both cases, as-deposited or light-soaked, we observe a degradation of the transport parameters when the sample is set under vacuum and an improvement once put under air. With some samples we even observed a fully reversible evolution of L_d between air and vacuum environment[30] (see also Fig. S4). This behavior is in line with the PL spectra evolution recorded either under air or under vacuum.

Another interesting point is that, under light-soaking, the photoconductivity drops down while L_d remains almost constant. Indeed, this parameter is only reduced by ~ 22 %, a rather small decay compared to the drop by a factor of 10 of the photoconductivity compared to the values in the as-deposited state. Moreover, it can be noted that the decrease of the photoconductivity with light-soaking goes along with a decrease of the dark conductivity as shown in Fig. S5 of the supporting information.

We have repeated the same experiment on other films with similar trends (See Fig. S6). Once again, the diffusion length was almost not affected by the light-soaking process whereas a systematic decrease of the photoconductivity by a factor of 10 was noted.

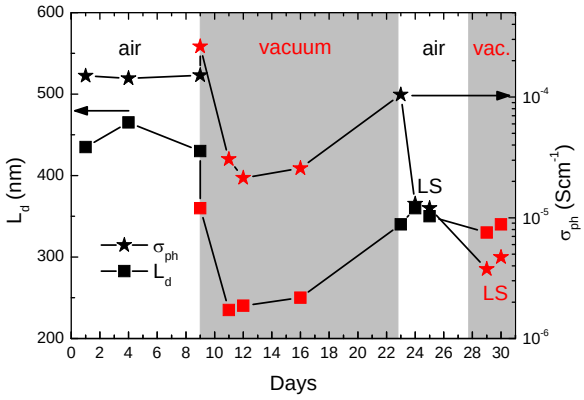

Figure 4. Evolutions of the ambipolar diffusion length L_d measured by SSPG (squares) and of the photoconductivity σ_{ph} measured by SSPC (stars) under different environments (air in black or vacuum in red) and with light-soaking (LS). Lines are guides to the eye.

Moreover, the evolutions of the photocurrent I_{ph} have been measured during light-soaking under air or under vacuum and are presented in Fig. 5. The trends are rather similar in both cases. After a slight decrease during the first minute we observe an increase of I_{ph} followed by another more pronounced decay. After one day of light soaking, I_{ph} reaches values ten times lower than the values in the as-deposited state, for both under air and under vacuum conditions.

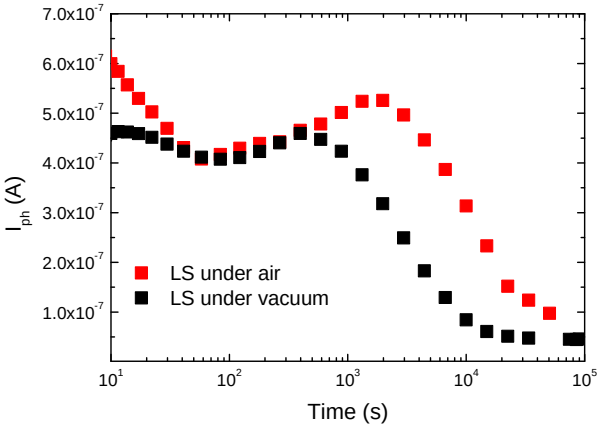

Figure 5. Photocurrent evolution during light-soaking (LS) of triple-cation PVK thin films under air (red squares) and under vacuum (black squares).

Finally, FTPS experiments have been carried out on different samples before and after light-soaking both under vacuum and under air. The results are presented in Fig. 6.

It can be seen that there is only little evolution of the FTPS spectrum when light-soaking is done under vacuum. However, we can estimate an average increase of the deep states by a factor around 2. When light-soaking is done under air we observe a red shift of the band gap, the Urbach tail being moved to lower energies (see the black and dark yellow curves of Fig. 6(b)). To have a better overview of the deep states increase, the FTPS spectrum obtained after light-soaking has been plotted 40 meV upward to match the band tail of the FTPS spectrum obtained in the as-deposited state (dashed red curve of Fig. 6(b)). This shift puts into evidence that the band tail of the density of states is not modified by light-soaking and underlines a slight increase of the deep states by a factor of 2 to 3 around 1.35 eV. We have also investigated on the reversibility of the band gap evolution. With the FTPS experiment, we have observed that the bang gap comes back to its initial position if the sample is left under dark and under primary vacuum at room temperature within a few days. Example of such an evolution is presented in Fig. S7.

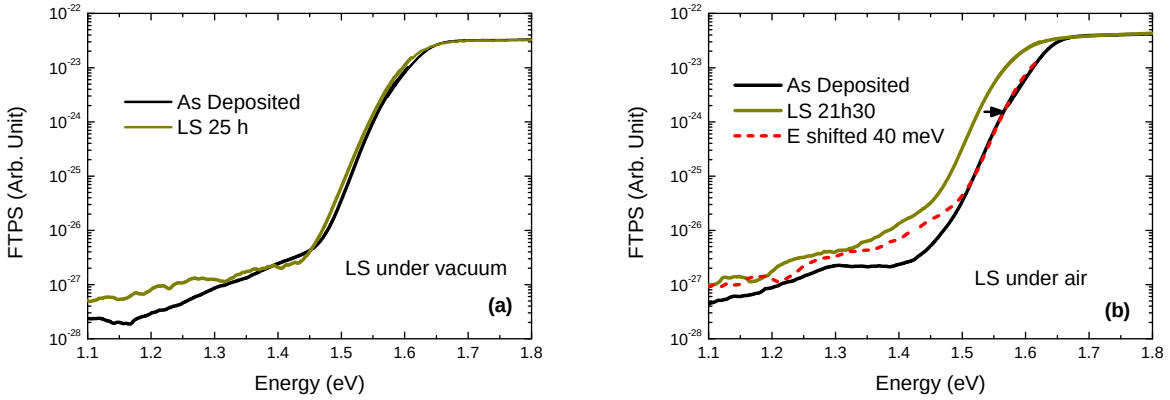

Figure 6. Evolution of the FTPS spectra with light soaking (a) performed under vacuum (b) performed under air. The FTPS spectrum obtained after light-soaking under air has been sifted 40 meV upward (dashed red line) to be compared with the as-deposited spectrum.

3. DISCUSSION

Before going further in the discussion of the PL results we would like to underline the influence of the wavelength on the penetration depth of the light. Shorter wavelengths are absorbed closer to the surface than the longer ones. Measurements by ellipsometry of the absorption coefficient α of our triple-cation perovskite have shown that α(470 nm) $\approx 2\times10^5$ cm^{-1} and α(670 nm) $\approx 3.2\times10^4$ cm^{-1} which means that the penetration depths of the light are around 50 nm and 310 nm for 470 nm and 670 nm, respectively.

The rise of the PL response, when done with short illumination times (ON/OFF PL) (See Figs. 1-2), is certainly due to the passivation of non-radiative traps starting from the very top surface of the film in contact with the atmosphere, in line with the results presented in the literature.[17, 18] Assuming that the passivation depends on the penetration of an air component inside the film, the passivation depth must be time dependent. In this case, passivation must occur in two steps, each needing a certain amount of time: the time for the air to penetrate the film and the time linked to the kinetic of the passivation reaction itself. The experimental results we obtained tend to confirm this assumption. Indeed, since the blue laser is absorbed very close to the surface, the influence of the passivation of the very first layers of the film is faster for the PL response at 470 nm than for the red laser which is absorbed deeper in the film.

The reversible creation of a passivation layer on top of the PVK film may also explain one of the evolutions of transport properties of the samples. When exposed to the air, the creation of a passivation layer on top of the film should result in the decrease of a recombination path and eventually in an increase of the carrier lifetimes, explaining the increase of the photoconductivity (see also Fig. S8 of the supporting information) and diffusion length experimentally measured.

However, when the PL spectra are recorded under air with a continuous illumination by the lasers light (Figs. S1(a), S1(c)), we still observe an increase of the PL intensity but with much longer time constants and accompanied by a red-shift of the PL maximum. This result is consistent with recent observation of a red-shift of the PL maximum during light-soaking in air for triple-cation PVK by Andaji-Garmaroudi and coworkers.[31] This is also consistent with the shrinking of the band gap (see Figs. 3(b) and 6(b)) measured during the light-soaking study, suggesting the same type of degradation. The continuous illumination of the lasers light induces the same red-shift of the gap, identified by the red-shift of the PL peak, as if the films were light-soaked, at least partially, during the experiment. We cannot therefore reject a possible competition between passivation, which increases the PL response, and degradation of the transport properties that slows down the PL intensity rise, this competition resulting in longer time constants for the increase of the PL maximum.

Finally, when the film is put under vacuum the decays of PL_{max} present the same time constants for the two tested wavelengths (Fig. 2). This results suggests that as soon as the film is set under vacuum, the desorption of the air passivating component (water vapor, oxygen,…) ”reactivate” the non-radiative recombining states and induces a rapid decrease of the PL intensity. In the case where the PL is measured under a steady illumination we do not observe a reversible evolution of the energy position of the PL maximum. This difference can be explained by the very long time constant, a few days, needed for the band gap to come back to its original value after light-soaking (See Fig. S7). The few minutes under which the evolution under vacuum of PL was observed are too short for the band gap to recover. Concerning this band gap shift, the reader may note that evolutions of the band gap under light-soaking and recovery after light-soaking have been reported in the literature with rather large time constants and have been attributed to phase segregation.[32, 33] However, we cannot definitely attribute the band gap shift observed in our case to this phenomenon since the

reported results concern PVK with much higher bromide content than in our samples and we do not observe any band gap shift when light-soaking is achieved under vacuum.

Concerning the opto-electronic properties, we observe under long light-soaking: i/ an increase of the photoluminescence, ii/ almost a stability of the diffusion length and iii/ a large decay of the photoconductivity. If one assumes that one type of carrier is predominant, the mobility×lifetime product of the majority carriers can be estimated from the expression of σ_{ph} and that of the minority carriers can be estimated from the expression of L_d given by[27]

$$\sigma_{ph} = q\,\eta(\mu\tau)_\sigma(1\text{-}R)\,F\,\alpha \qquad \text{and} \qquad L_d = \sqrt{2\frac{k_bT}{q}(\mu\tau)_L} \quad , \qquad (1)$$

where q is the absolute value of the electron charge, η is the quantum efficiency, $\mu\tau$ the mobility×lifetime products, R the reflection coefficient, k_b the Boltzmann constant and T the temperature. From the data of Fig. 4, before light-soaking, $\sigma_{ph} \approx 1.4\times10^{-4}$ Scm^{-1}, $L_d \approx 450$ nm, the $\mu\tau$ products can be estimated to be $(\mu\tau)_\sigma = 1.4\times10^{-6}$ cm^{2}V^{-1} and $(\mu\tau)_L = 4.0\times10^{-8}$ cm^{2}V^{-1} at room temperature. After light-soaking, $\sigma_{ph} \approx 1.2\times10^{-5}$ Scm^{-1}, $L_d \approx 350$ nm, giving $(\mu\tau)_\sigma = 1.3\times10^{-7}$ cm^{2}V^{-1} and $(\mu\tau)_L = 2.4\times10^{-8}$ cm^{2}V^{-1}. It can be seen that, in both states of the film, before and after light-soaking, we always have $(\mu\tau)_\sigma$ much larger than $(\mu\tau)_L$ meaning that indeed one type of carrier dominates the transport. In addition, after light-soaking, $(\mu\tau)_\sigma$ has decreased by a factor of the order of 10. If one assumes that this decay is essentially due to a decrease of τ, it would mean that a recombination path had widened resulting from an increase of the deep defect density of states.

However, the results obtained from FTPS invalidate this assumption. According to the spectra evolution upon light-soaking (See Fig. 6) the deep defect density increases by only a factor of 2 to 3 either when light-soaking is achieved under vacuum or under air: the spectra displayed in Fig. 6 emphasize the small deep states evolution with light-soaking. We cannot reject the possibility of an increase of deep states below 1.1 eV but, even in this case, it would

be difficult to understand that if the decrease of $(\mu\tau)_\sigma$ by a factor of 10 was only due to a decay of τ, we also observe: i/ a diffusion length only very little affected by this enhanced recombination path, and, ii/ an increase by a factor of 2 of PL_{max} after light-soaking. Remembering that without light-soaking we have obtained, under air, an increase of the PL maximum by a factor of 3 that we have attributed to surface passivation, the increase by a factor of 2 under light-soaking could be also due to a surface passivation effect mitigated by a small degradation of the lifetime. These results suggest that the observed decrease of $(\mu\tau)_\sigma$ is more probably a combined effect of a (small) decrease of the lifetime and a (large) decrease of the mobility of the majority carriers according to [34].

As seen with the above results we are systematically dealing with a competition between passivation and degradation during light-soaking, and this competition influences the transport properties as illustrated in Fig. 5. At short times, the photocurrent (I_{ph} = 6.1×10^{-7} A) for the sample under air is higher than for the sample under vacuum (I_{ph} = 4.5×10^{-7} A) and both decrease under the influence of the degradation due to light-soaking. In a second region, after 80 s of light-soaking, the photocurrent starts to increase, in a less pronounced manner and during a shorter period of time for the sample under vacuum (~ 10 % at t ≈ 400 s) than under air (~ 32 % at t ≈ 1600 s). Then in a third region, both photocurrents decrease to reach quite similar values around I_{ph} = 4×10^{-8} A. These behaviors reflect the competition between passivation and degradation during light-soaking. Light-soaking induces first a degradation of the transport properties in region 1 for both films (under air and under vacuum). Then, passivation of the surface occurs, mainly for the sample in contact with air, until degradation takes the pace over passivation in the third region. Fig. 7 summarizes the competition between passivation and degradation during light-soaking, these two processes presenting very different time constants, rather short for the passivation and quite long for the degradation.

On the contrary the degradation mechanism only weakly influences the PL intensity, suggesting again that it mainly affects the mobility of the majority carriers instead of their lifetime.

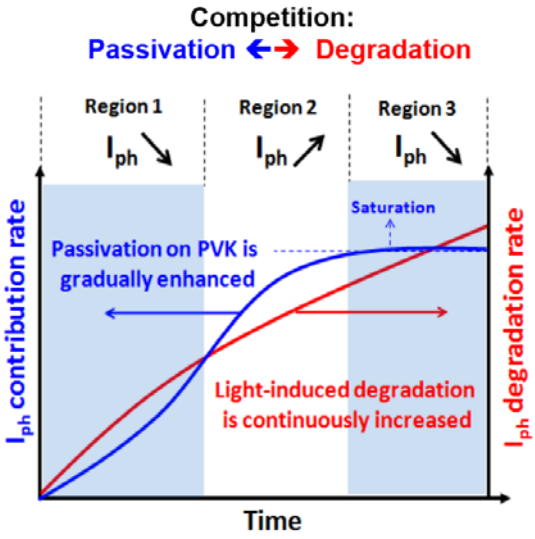

Figure 7. Schematic diagram of the competition between passivation and degradation during light-soaking and its influence on the photocurrent.

We would like to add a few comments on this competition between passivation and degradation that could give also some directions for future research studies. The first one deals with the nature of the passivation mechanism. It can be due to a chemical reaction or to simple adsorption which might be either physisorption or chemisorptions. In the case of physisorption the reversibility can be easily explained. Indeed, physisorption would concern only few nanometers at the perovskite top interface (PVK/air) with rather weak bonding (Van der Walls bonding, for instance) and desorption would be induced almost instantaneously when the sample is set under vacuum. In case of chemisorption, the created bonds would be stronger and reversibility would imply an extra source of energy such as the temperature (heat) of the sample. In this last case, the phenomenon should be activated with temperature but such a study was largely beyond the scope of the paper.

The second point deals with the influence of the light in the mechanisms of passivation and degradation. Concerning this latter, light seems to induce degradation both under vacuum and under air. The mechanism that can be responsible for defect creation by light is the following. By band to band generation light creates free carriers that recombine either radiatively or non-radiatively. In the second case, the energy lost during recombination is transmitted to the network and can be enough to break weak bonds or initiate chemical reactions and eventually to create defects. The degradation would be faster under vacuum because the passivation of the top surface of PVK by air is absent which is precisely one of our observations. Concerning this passivation or rather de-passivation, light may provide additional energy to de-passivate the PVK/air interface when the sample is set under vacuum from the same mechanism as exposed above. Thus, light would also work against the passivation when the sample is set under air. It could be an alternative explanation to the different time constants we found, larger for passivation than for de-passivation.

4. CONCLUSIONS

We have investigated on the influence of the environment and light-soaking onto the opto-electronic and transport properties of triple-cation perovskite thin films. For that purpose, we have applied several complementary characterization techniques - photoluminescence, Fourier transform photocurrent spectroscopy, steady state photocarrier grating, dark and photoconductivity - to thin films maintained either under air or under vacuum. Air exposure resulted into an increase of the PL peak intensity, of the diffusion length and of the photoconductivity. We have suggested that this improvement is due to the creation of a passivation layer on top of the PVK film, this creation taking place within a few minutes after exposure to air.

More surprising are the results obtained after light-soaking since we have observed an increase of the PL maximum accompanied by a red-shift of its energy position, a small decrease of the diffusion length but a large decrease of the photoconductivity by a factor of the order of 10. Using FTPS we have shown that light-soaking under air produced a shrinking of the gap by the same amount of the red-shift of the PL maximum. Though phase segregation could be thought to be at the origin of this gap reduction, this process does not explain why such a reduction is not seen when the film is light-soaked under vacuum. We may suggest a deep penetration of an air component inside the material by diffusion, a process that would also explain the long time needed for the band gap to recover its as-deposited value, the time needed for the complete exo-diffusion of this component. FTPS has also shown that the deep defect density, at least above 1.1 eV, was only little affected by light-soaking. Therefore, the origin of the decrease of the photoconductivity cannot be completely attributed to a decrease of the carrier lifetime that would be linked to an increase of the deep defect density, unless this increase occurs below 1.1 eV and is undetected by FPTS. However, in this last case we should have observed a large degradation of the diffusion length which is not the case. We believe then that light-soaking induces mostly a decay of the majority carrier mobility, a process that would unaltered the diffusion length linked to the minority carriers and that would have only little influence on the PL spectra, the maximum of which increase under air even during light-soaking.

This last result underlines the competition that exists between improvement of the opto-electronic properties by passivation by air of the film surface and the degradation of some of these properties under light-soaking.

5. EXPERIMENTAL SECTION

5.1. Perovskite films deposition. The perovskite (PVK) thin layers in this study were

composed of three cations, Methylammonium (MA), Formamidinium (FA), and Cesium (Cs). To grow the perovskite films, a double-cation perovskite solution, $(MA_{0.17}FA_{0.83})Pb(Br_{0.17}I_{0.83})_3$ referred as $(MA,FA)Pb(Br,I)_3$, was first prepared by dissolving 1.10 M PbI_2 (TCI Chemicals), 0.20 M $PbBr_2$ (Alfa Aesar), 1.00 M formamidinium iodide (FAI, Dyesol) and 0.20 M methylammonium bromide (MABr, Dyesol) in a mixture of DMSO:DMF (4:1 in v/v) as solvent. In order to obtain the three cations perovskite, i.e. $Cs_x(MA_{0.17}FA_{0.83})_{1-x}Pb(Br_{0.17}I_{0.83})_3$, the required quantity of Cs^+ was additionally injected from a precursor solution of CsI (Sigma Aldrich) 1.50 M in DMSO solvent.[35] After stirring in a magnetic mixer for ~18 hours, the mixed perovskite solution was then deposited on glass substrates by spin-coating, utilizing a double plateau (2000 rpm to cast the perovskite precursor solution followed by 6000 rpm to drip 100 µL of chlorobenzene). The 1 mm thick glass substrates were rinsed in solutions of acetone, ethanol, and followed by exposure to an UV-ozone cleaner for 120 min just before spin-coating. After deposition, the perovskite films were submitted to an annealing treatment at a temperature of 100 °C for 30 minutes in a N_2 glove box. The perovskite films had an average thickness ~ 500 nm, and their morphology, measured via SEM, showed that compact films were obtained with a crystalline grain size in the range 200 - 400 nm. The finalized thin films were then fitted with two parallel Au electrodes, 1.5 mm apart and 1 cm long, deposited by thermal evaporation. A SEM cross-section picture of a device incorporating a typical PVK film and a SEM top view of a PVK film are given in Figs. S9 and S10, respectively, showing the morphological structure of the PVK films we have studied. Fig. S11 displays an $I(V)$ curve obtained on one of our PVK devices

5.2. Opto-electronic characterizations. Optical properties of the films were investigated with photoluminescence (PL) and Fourier transform photocurrent spectroscopy (FTPS) experiments. Photoluminescence measurements were performed the samples being set into a

cryostat either under atmospheric conditions or under a vacuum level below 10^{-5} mBar. Optical excitation was achieved by two continuous diode lasers with wavelengths of 470 nm (Power density 0.83 Wcm^{-2}) and 670 nm (Power density 1.41 Wcm^{-2}) with an illumination making an angle of 30° with the sample surface. PL emission was collected by a lens and an optical fiber positioned 10 cm in front of sample and was then analyzed with a spectrometer to obtain the PL spectrum. By using a shutter in between the laser beams and the sample, we could control the illumination time to just a few seconds, long enough to record the PL spectrum but short enough to avoid a possible degradation of the PVK sample by a continuous illumination (ON/OFF PL experiment). In addition, some PL experiments were done with a steady illumination of the film by the lasers light.

The Fourier transform photocurrent spectroscopy was proposed a few years ago to measure the variations of the absorption coefficient α of semiconductor thin films with a below gap photon energy.[22, 23] Since this absorption is mainly linked to transition from occupied states toward empty states this technique also gives information on the density of states (DOS) responsible for the observed absorption and its possible evolution under some external constraints like submission to strong illumination (light-soaking). It must be underlined that FTPS provides only relative variations of α with the photon energy. To obtain the absolute variations of α the FTPS spectrum has to be calibrated from transmission/reflection measurements. For a review of the FTPS technique and its application to thin films see for instance the work of J. Holovski.[36]

The transport properties of the films were investigated with dark conductivity, steady state photoconductivity (SSPC), and steady state photocarrier grating (SSPG) experiments. The dark photoconductivity and SSPC are standard characterization techniques but the SSPG is a more sophisticated technique used to derive the ambipolar diffusion length of the carriers in semi-insulating materials.[24, 27, 37]

In the SSPG experiment a light beam coming out of a He-Ne laser (632.8 nm) with a polarization parallel to the electrodes is split into two beams subsequently sent onto the sample in between the electrodes to superimpose one over the other making an angle θ between them. One of the beams can be considered as the main one since it fixes the steady state of the sample. The other beam, the probe beam, is attenuated by a factor of the order of 30 and generates a small perturbation of the steady state of the sample. A voltage bias is applied in between the electrodes and one measures the excess current flowing through the sample resulting from this perturbation. Two cases can be considered. If the light polarization of both beams is parallel to the electrodes, the superimposition of the beams results in the generation of interferences on and in the film with a grating period Λ depending on the angle θ. In this case one measures an excess current I_w. If the light polarization of one beam, for instance the main one, is rotated by a $\lambda/2$ plate so that the beam polarizations are crossed, the two light beams simply superimpose and one measure a current I_{wo}. It was shown by Ritter and co-workers that the ratio $\beta=I_w/I_{wo}$ depends on the grating period and on the ambipolar diffusion length via the expression[24]

$$\beta(\Lambda) = 1 - \frac{2\phi}{\left[1+\left(\frac{2\pi L_d}{\Lambda}\right)^2\right]^2} \quad , \qquad (2)$$

where ϕ is a parameter that depends on the conductivity of the material and the quality of the interferences, and L_d is the ambipolar diffusion length. Consequently, after measurement of β with different angles between the beams, and thus with different Λ, a fitting of the $\beta(\Lambda)$ curve with Eq. (2) provides information on the carrier ambipolar diffusion length.

The 'classical' SSPG bench has been largely improved.[29] The modification of the angle between the beams was fully automated and a cryostat was added to study thin film ambipolar diffusion length, the sample being either in the air or under vacuum at different temperatures. The same bench can also be used to perform under the same conditions as SSPG (same flux,

same environment, same temperature) either dark conductivity or photoconductivity (SSPC) measurements.

Light-soaking of the samples was achieved under air or under vacuum with a high power LED presenting a spectrum close to that of AM1.5G illumination in the visible range with a power density of 44 $mWcm^{-2}$. A comparison of the AM1.5G spectrum and of the high power LED spectrum can be found in Fig. S3 of the supporting information. The fact that there is no infra-red component in the LED spectrum is not detrimental to the light-soaking effect since the light is only weakly or even not absorbed by the PVK film for wavelengths larger than 800 nm. The advantage of the high-power LED is the lack of infra-red wavelengths which avoid heating of the sample during light-soaking. Indeed, using a thermal camera we have observed that under the LED flux the sample temperature was only increasing from 23 °C to 28 °C. Therefore, we could rule out any influence of the temperature on the phenomena we have observed.

ASSOCIATED CONTENT

Supporting information

PL under steady illumination, Light-soaking spectrum, Evolution of L_d under air and under vacuum, Evolution of the Arrhenius plots of dark and photo conductivity under light-soaking, Evolution of band gap with light-soaking and recovery, Evolution of the photocurrent under air and vacuum, Morphology of the PVK thin films, I(V) curves.

AUTHOR INFORMATION

Corresponding author

* E-mail : longeaud@geeps.centralesupelec.fr

Author contribution

The manuscript was written through contributions of all authors. All authors have given approval to the final version of the manuscript.

Notes

The authors declare no competing financial interest.

ACKNOWLEDGEMENTS

This project has been supported by the French Government in the frame of the program of investment for the future (Program d'Investissement d'Avenir - ANRIEED-002-01). S.C. thanks funding from the European Union's Horizon 2020 research and innovation program under the Marie Skłodowoska-Curie Grant Agreement N° 845612. Many thanks to D. Loisnard for the SEM measurements, E. Raoult for the ellipsometry data and A Yaiche, S. Bgegnon and A. Duchatelet for the *I*(*V*) studies.

Table of Content graphic

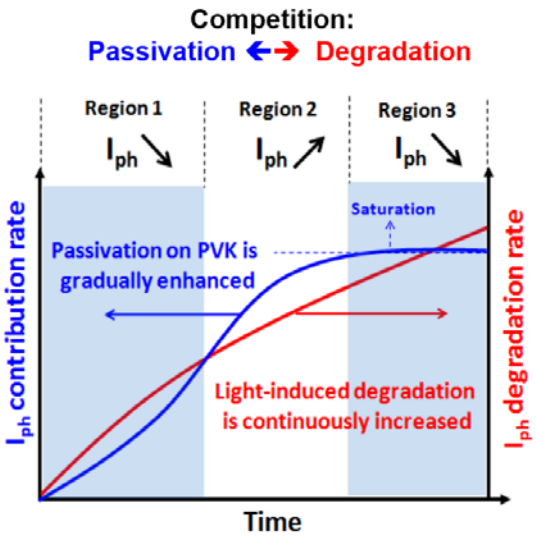

REFERENCES

(1) Chen, Q.; De Marco, N.; Yang, Y. M.; Song, T.-B.; Chen, C.-C.; Zhao, H.; Hong, Z.; Zhou, H.; Yang, Y. Under the Spotlight: The Organic-Inorganic Hybrid Halide Perovskite for Optoelectronic Applications. *Nano Today* **2015,** *10*, 355-396.

(2) Boix, P. P.; Nonomura, K.; Mathews, N.; Mhaisalkar, S. G. Current Progress and Future Perspectives for Organic/Inorganic Perovskite Solar Cells. *Materials Today* **2014**, *17*, 16-23.

(3) Tan, H.; Jain, A.; Voznyy, O.; Lan, X.; Pelayo García de Arquer, F.; Fan, J. Z.; Quintero-Bermudez, R.; Yuan, M.; Zhang, B.; Zhao, Y.; Fan, F.; Li, P.; Quan, L. N.; Zhao, Y.; Lu, Z.-H.; Yang, Z.; Hoogland, S.; Sargent, E. H. Efficient and Stable Solution-Processed Planar Perovskite Solar Cells via Contact Passivation. *Science* **2017**, *355*, 722–726.

(4) Kojima, A.; Teshima, K.; Shirai, Y.; Miyasaka, T. Organometal Halide Perovskites as Visible-Light Sensitizers for Photovoltaic Cells. *J. Am. Chem. Soc.* **2009**, *131*, 6050-6051.

(5) NREL. Research Cell Record Efficiency Chart. https://www.nrel.gov/pv/cell-efficiency.html (accessed August 2019).

(6) Tan, Z. K.; Moghaddam, R. S.; Lai, M. L.; Docampo, P.; Higler, R.; Deschler, F.; Price, M.; Sadhanala, A.; Pazos, L. M.; Credgington, D.; Hanusch, F.; Bein, T.; Snaith, H. J.; Friend, R. H. Bright Light-Emitting Diodes Based on Organometal Halide Perovskite. *Nat. Nano.* **2014**, *9*, 687-692.

(7) Xing, G.; Mathews, N.; Lim, S. S.; Yantara, N.; Liu, X.; Sabba, D.; Grätzel, M.; Mhaisalkar, S.; Sum, T. C. Low-Temperature Solution-Processed Wavelength-Tunable Perovskites for Lasing. *Nat. Mater.* 2014, *13*, 476-480.

(8) Sutherland, B. R.; Hoogland, S.; Adachi, M. M.; Wong, C. T.; Sargent, E. H. Conformal Organohalide Perovskites Enable Lasing on Spherical Resonators. *ACS Nano* **2014**, *8*, 10947-10952.

(9) Dou, L.; Yang, Y. M.; You, J.; Hong, Z.; Chang, W.-H.; Li, G.; Yang, Y. Solution-Processed Hybrid Perovskite Photodetectors with High Detectivity. *Nat. Commun.* **2014**, *5*, 5404.

(10) Xia, H.-R.; Li, J.; Sun, W.-T.; Peng, L.-M. Organohalide Lead Perovskite Based Photodetectors with much Enhanced Performance. *Chem. Commun.* **2014**, *50*, 13695 - 13697.

(11) Kwon, Y. S.; Lim, J.; Yun, H.-J.; Kim, Y.-H.; Park, T. A Diketopyrrolopyrrole-Containing Hole Transporting Conjugated Polymer for Use in Efficient Stable Organic–Inorganic Hybrid Solar Cells Based on a Perovskite. *Energy Environ. Sci.* **2014**, *7*, 1454-1460.

(12) Wang, X.; Xinxin Zhao, C.; Xu, G.; Chen, Z.-K.; Zhu, F. Degradation Mechanisms in Organic Solar Cells: Localized Moisture Encroachment and Cathode Reaction. *Solar Energy Materials and Solar Cells* 2012, *104*, 1-6.

(13) Madogni, V. I.; Kounouhéwa, B.; Akpo, A.; Agbomahéna, M.; Hounkpatin, S. A.; Awanou, C. N. Comparison of Degradation Mechanisms in Organic Photovoltaic Devices upon Exposure to a Temperate and a Subequatorial Climate. *Chemical Physics Lett.* **2015,** *640*, 201-214.

(14) Heo, S.; Seo, G.; Lee, Y.; Seol, M.; Kim, S. H.; Yun, D. J.; Kim, Y.; Kim, K.; Lee, J.; Lee, J.; Jeon, W. S.; Shin, J. K.; Park, J.; Lee, D.; Nazeeruddin, M. K. Origins of High Performance and Degradation in the Mixed Perovskite Solar Cells. *Adv. Mater.* **2019**, *31*, 1805438.

(15) Motti, S. G.; Meggiolaro, D.; Martani, S.; Sorrentino, R.; Barker, A. J.; Angelis, F. D.; Petrozza, A. Defect Activity in Metal–Halide Perovskites. *Adv. Mater.* **2019**, *31*, 1901183.

(16) Senocrate, A.; Acartürk, T.; Kim, G. Y.; Merkle, R.; Starke, U.; Grätzel, M.; Maier, J. Interaction of Oxygen with Halide Perovskites. *J. Mater. Chem. A* **2018**, *6*, 10847-10855.

(17) Motti, S. G.; Gandini, M.; Barker, A. J.; Ball, J. M.; Srimath Kandada, A. R.; Petrozza, A. Photoinduced Emissive Trap States in Lead Halide Perovskite Semiconductors. *ACS Energy Lett.* **2016**, *1*, 726−730.

(18) Fang, H.-H.; Adjokatse, S.; Wei, H.; Yang, J.; Blake, G. R.; Huang, J.; Even, J.; Loi, M. A. Ultrahigh Sensitivity of Methylammonium Lead Tribromide Perovskite Single Crystals to Environmental Gases. *Sci. Adv.* **2016**, *2*, e1600534.

(19) Aristidou, N.; Eames, C.; Sanchez-Molina, I.; Bu, X.; Kosco, J.; Islam, M. S.; Haque, S. A. Fast Oxygen Diffusion and Iodide Defects Mediate Oxygen-Induced Degradation of Perovskite Solar Cells. *Nature communications* **2017,** *8*, 15218.

(20) Brenes, R.; Guo, D.; Osherov, A.; Noel, N. K.; Eames, C.; Hutter, E. M.; Pathak, S. K.; Niroui, F.; Friend, R. H.; Islam, M. S.; Snaith, H. J.; Bulović, V.; Savenije, T. J.; Stranks, S. D. Metal Halide Perovskite Polycrystalline Films Exhibiting Properties of Single Crystals. *Joule* **2017**, *1*, 155–167.

(21) Saliba M.; Matsui T.; Seo J.-Y.; Domanski K.; Correa-Baena J.-P.; Nazeeruddin M. K.; Zakeeruddin S. M; Tress W.; Abate A.; Hagfeldt A.; Grätzel M. Cesium-Containing Triple Cation Perovskite Solar Cells: Improved Stability, Reproducibility and High Efficiency *Energy Environ. Sci.* **2016**, *9*, 1989-1997.

(22) Poruba, A.; Vaněček, M.; Rosa, J.; Feitknecht, L.; Wyrsch, N.; Meier, J.; Shah, A.; Repmann, T.; Rech, B. Fourier Transform Photocurrent Spectroscopy in Thin Film Silicon Solar Cells. *Proc. of the 17th European Photovoltaic Solar Energy Conference*, **2001**, edited by WIP, Munich, Germany, p. 2981.

(23) Vaněček, M.; Poruba, A. Fourier Transform Photocurrent Spectroscopy of Micro-Crystalline Silicon for Solar Cells. *Appl. Phys. Lett.* **2002**, *80*, 719.

(24) Ritter, D.; Zeldov, E.; Weiser, K. Steady State Photocarrier Grating Technique for Diffusion Length Measurement in Photoconductive Insulators. *Appl. Phys. Lett.* **1986**, *49*, 791.

(25) Hodes, G.; Kamat, P. V. Understanding the Implication of Carrier Diffusion Length in Photovoltaic Cells. *J. Phys. Chem. Lett.* **2015**, *6*, 4090-4092.

(26) Adhyaksa, G. W. P.; Veldhuizen, L. W.; Kuang, Y.; Brittman, S.; Schropp, R. E. I.; Garnett, E. C. Carrier Diffusion Lengths in Hybrid Perovskites: Processing, Composition, Aging, and Surface Passivation Effects. *Chem. Mater.* **2016**, *28*, 5259-5263.

(27) Brüggemann, R. Steady State Photocarrier Grating Technique for the Minority-Carrier Characterisation of Thin-Film Semiconductors. *J. Phys.: Conf. Ser.* **2010**, *253*, 012081.

(28) Veldhuizen, L. W.; Adhyaksa, G. W. P.; Theelen, M.; Garnett, E. C.; Schropp, R. E. I. Benchmarking Photoactive Thin Film Materials Using a Laser Induced Steady State Photocarrier Grating. *Progress in Photovoltaics* **2016**, *25*, 605-613.

(29) Longeaud, C. An Automated Steady State Photocarrier Grating Experiment. *Rev. Sci. Instrum.* **2013**, *84*, 055101.

(30) Longeaud, C.; Ramos, F. J.; Rebai, A.; Rousset, J. Impact of Environmental Stresses Onto Transport Properties of Hybrid Perovskite Investigated by Steady State Photocarrier Grating and Steady State Photocurrent Techniques. *Sol. RRL* **2018**, *2*, 1800192.

(31) Andaji-Garmaroudi Z.; M. Abdi-Jalebi M.; Guo D.; Macpherson S.; Sadhanala A.; Tennyson E. M.; Ruggeri E.; Anaya M.; Galkowski K.; Shivanna R.; Lohmann K.; Frohna K.; Mackowski S.; Savenije T. J.; Friend R. H.; Stranks S. D. A Highly Emissive Surface Layer in Mixed-Halide Multication Perovskites *Adv. Mater*. **2019**, *31*, 1902374.

(32) Barker, A. J.; Sadhanala, A.; Deschler, F.; Gandini, M.; Senanayak, S. P.; Pearce, P. M.; Mosconi, E.; Pearson, A. J.; Wu, Y.; Ram Srimath Kandada, A.; Leijtens, T.; De Angelis,

F.; Dutton, S. E.; Petrozza, A.; Friend, R. H. Defect-Assisted Photoinduced Halide Segregation in Mixed-Halide Perovskite Thin Films. *ACS Energy lett.* **2017**, *2*, 1416.

(33) Brennan, M. C.; Dragutta, S.; Kamat, P. V.; Kuno, M. Light-Induced Anion Phase Segregation in Mixed Halide Perovskites. *ACS Energy lett.* **2018**, *3*, 204.

(34) Guo, D.; Andaji-Garmaroudi, Z.; Abdi-Jalebi, M.; Stranks, S. D.; Savenije, T. J. Reversible Removal of Intermixed Shallow States by Light Soaking in Multication Mixed Halide Perovskite Films. *ACS Energy lett.* **2019**, *4*, 2360-2367.

(35) Saliba, M.; Matsui, T.; Seo, J.-Y.; Domanski, K.; Correa-Baena, J.-P.; Mohammad, N. K.; Zakeeruddin, S. M.; Tress, W.; Abate, A.; Hagfeldt, A.; Grätzel, M. Cesium-Containing Triple Cation Perovskite Solar Cells: Improved Stability, Reproducibility and High Efficiency. *Energy Env. Sci.* **2016**, *9*, 1989.

(36) Holovsky, J. in Fourier Transforms-New Analytical Approaches and FTIR Strategies, edited by G. Nikolic (IntechOpen, **2011**), Chap. 13

(37) Ritter, D.; Weiser, K.; Zeldov, E. Steady State Photocarrier Grating Technique for Diffusion-Length Measurement in Semiconductors: Theory and Experimental Results for Amorphous Silicon and Semi-Insulating GaAs. *J. Appl. Phys.* **1987**, *62*, 4563.